Journal of Materials Chemistry A

Accepted Manuscript

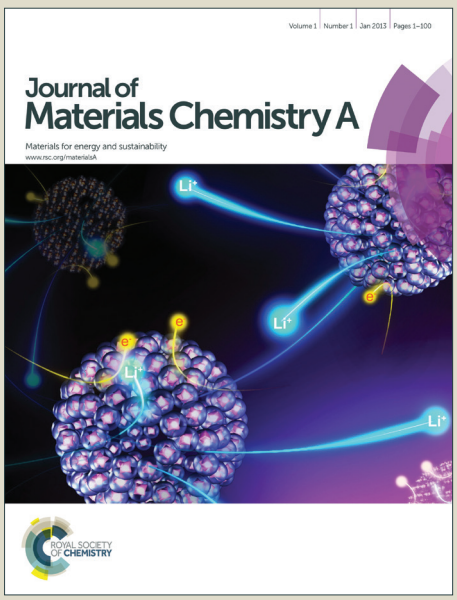

ROYAL SOCIETY OF CHEMISTRY

www.rsc.org/materialsA

Hetero-Structured $TiO_2/SrTiO_3$ Nanotube Array Film with High-Reactive Anatase TiO_2 {001} Facets

Juan-Ru Huang,[a,b] Xin Tan, [a,b] Tao Yu[*, a,c], Lin Zhao,[b] Song Xue,[d] Wen-Li Hu[b]

[a]School of Chemical Engineering and Technology, Tianjin University, Tianjin, 300072, China

[b]School of Environmental Science and Engineering, Tianjin University, Tianjin, 300072, China

[c]Tianjin University-National Institute for Materials Science Joint Research Center, Tianjin University, Tianjin, 300072, China

[d]Department of Applied Chemistry, Tianjin University of Technology, Tianjin, 300191, China

***Corresponding Author**: Yu Tao, Huang Juan-Ru

Tel.: 86-22-2350-2142. E-mail: yutao@tju.edu.cn, huangjuanru@tju.edu.cn

ABERSTRACT: In recent years, highly reactive anatase TiO_2 with controllable facets has expanded rapidly because its unique properties provides a new sight of interfacial chemistry to TiO_2 as photocatalyst, electrode materials and so on. Herein, we develop for the first time to fabricate hetero-structured $TiO_2/SrTiO_3$ nanotube arrays with the preferred orientation to anatase TiO_2 {001} facet by a typical anodization and subsequent hydrothermal approach, followed by an annealing process. Based on XRD, FE-SEM, FE-TEM, XPS and Raman measurement, partial TiO_2 is successfully converted into $SrTiO_3$ attached on in-situ TiO_2 nanotubes and the hetero-structured interface of $TiO_2/SrTiO_3$ with preferred growth of anatase TiO_2 {001} facet is definitely formed after hydrothermal process. In addition, the resulting hetero-structured samples are used as the photocatalyst to decolorize "target molecular" methylene blue (MB) of aqueous solution in a photocatalytic and photoelectrocatalytic process, and the hetero-structured samples reveal enhanced photocatalytic properties compared to the reference TiO_2 nanotube arrays.

KEYWORDS High-Reactive, TiO_2 {001} facet, Hetero-Structured Nanotube Arrays, Photocatalysis, Photoelectrocatalysis

The Design and fabrication of anatase TiO_2 nanostructures have attracted much attention because of their extensive application in photocatalysis,[1-3] dye-sensitized solar cell,[4, 5] sensors and related fields.[6, 7] Previous work mainly focused on the most prevalent anatase TiO_2 with the thermodynamically stable {101} (up to 94%) and minor {001} facets due to the minimization of average surface energy during the crystal growth processes under equilibrium conditions, which is described to the calculated surface energy (0.44 J/m^2 for {101} < 0.53 J/m^2 for {100} = {010} < 0.90 J/m^2 for {001}) based on Wulff construction and density-functional theory (DFT) calculations,[8, 9] and the calculations[8] also deduce that these facets with under-coordinated five-fold Ti atoms (Ti_{5c}) possess superior reactivity than that of Ti_{4c} and, thereby, {001} and {100} facets with 100% Ti_{5c} manifest high activity based on the lattice structure of anatase TiO_2. A breakthrough work is acquired to fabricate anatase TiO_2 single crystals with dominant {001} facet using HF as a capping agent under hydrothermal conditions.[10] Subsequently, the related investigation employ large doze-ratio fluoride to promote high-active facets and then enhance the photo-generated electron transport to improve photocatalytic activity,[1, 11-20] and the free-fluorine synthetic strategies with H_2SO_4, gray mineral, carbonate ions and amine stimulate the oriented growth of specific facets and then synthesis anatase TiO_2 with dominant {001} facet.[2, 21-24] Recently, 1D TiO_2 nanotube arrays with the preferred growth of {001} facets, which are assembled via anodizing Ti substrate in a electrolyte containing F^-, investigated to enhance the photovoltaic performance since these high-reactive {001} facets and the structural advantage of 1D nanomaterials effectively reduce the combination of photo-generated electrons and holes.[25, 26]

The photochemical properties of semiconductor materials are determinated by the cooperative mechanism of surface atomic structure (the density of undercoordinated atoms) and surface electronic structure (the energy of photoexcited electrons),[19] which directly triggers the

increasing attempt to construct the coupling semiconductors,[3, 27-29] and then the resulting composite can generate enhanced photoelectrochemical properties compared with single semiconductor. In such an approach, the proper coupling of TiO_2 and $SrTiO_3$ bestow positive energetics and synergies in attaining spatial delocalization of photo-generated electrons and holes because of the unique energy band structure.[30] In particular, hetero-structured TiO_2/$SrTiO_3$ (TSr) nanotube arrays on a Ti substrate are successfully synthesized with using anodic TiO_2 nanotubes as a structure template and initial reactant in in-situ hydrothermal synthesis route, and a partial conversion of TiO_2 to $SrTiO_3$ on the surface of TiO_2 nanotubes is investigated to yield considerably improved photoelectrochemical properties in comparison to pure TiO_2 nanotubes.[31-36] Here, we firstly report a facile hydrothermal approach to directly grow hetero-structured TSr nanotube arrays with the preferred growth {001} facet of anantase TiO_2 adhered on a Ti substrate, using TiO_2 nanotube arrays by anodization as a "structure-directed" template and initial reactant, and the resulting hetero-structured film exhibits enhanced photocatalytic and electrochemical properties than reference TiO_2 (TSr_0) nanotube array film.

High-reactive hetero-structured TSr nanotube array film on a Ti (TSr/Ti) substrate is fabricated by a typical hydrothermal method, utilizing TiO_2 nanotube arrays as a template and initial reactant to generate the hetero-structured in a rational manner (experimental details, Electronic Supporting Information), and the reference TSr_0 nanotube array film with a Ti substrate (TSr_0/Ti) is synthesized according to our previous report[4]. The XRD patterns of the resulting hetero-structured TSr_{301}/Ti (the subscript represents that the hydrothermal concentration and time are 0.025 M $Sr(OH)_2$ and 30 min, respectively), TSr_{301}*/Ti ("*" points out this sample without annealing) and reference TSr_0/Ti, Ti samples are shown in Fig. 1a, the XRD patterns of TSr_0/Ti reveal that anatase TSr_0 with diffraction peaks at about $2\theta = 25.7^o$,

38.4°, 48.5°, 53.5°, 55.6°, 63.3°, 75.5° is perfectly indexed to the (101), (004), (200), (105), (211), (204), (115) facet of anatase TiO_2 (JCPDS No.75-1537), and the patterns of Ti substrate are in good accordance with the Ti (JCPDS No.44-1294). After the hydrothermal reaction, the XRD patterns of the TSr_{30}*/Ti sample illuminate that the several diffraction peaks at about 2θ = 33.0°, 47.1°, 58.4°, 68.5° are indexed to the crystal facets (110), (200), (211), (220) of perovskite $SrTiO_3$ (JCPDS No. 35-0734) and, thereby, confirm that part of TiO_2 is successfully converted into $SrTiO_3$ particles on the surface of "structure-directed" TiO_2 nanotubes by an in-situ dissolution-precipitation process,[35, 37] and this process is described to two steps: (1) The Ti-O bonds of the TiO_2 precursor are firstly broken via hydrolytic attack to from soluble $[Ti(OH)_6]^{2-}$ ($TiO_2 + 2OH^- + 2H_2O \rightarrow [Ti(OH)_6]^{2-}$), (2) Small $SrTiO_3$ particles, which originate from the Sr^{2+} of $Sr(OH)_2$ substituting for Ti^{2+} of $[Ti(OH)_6]^{2-}$, are precipitated on the surface of TiO_2 nanotubes ($Sr^{2+} + [Ti(OH)_6]^{2-} \rightarrow SrTiO_3 + 3H_2O$), thus the total reaction is expressed: $TiO_2 + Sr(OH)_2 \rightarrow SrTiO_3 + H_2O$. With the annealing at 450 °C, a sharp peak at about 2θ = 38.4° appears in the XRD patterns of TSr_{301}/Ti and is in good agreement with the preferred {001} facet of anatase TiO_2.[12, 19, 24, 25, 38]

Compared with the XRD patterns of the hetero-structured and reference samples, the bonding of $SrTiO_3$ on the "bone structure" of TiO_2 nanotubes in the hydrothermal process directly propels the oriented growth of anatase TiO_2 {001} facet in the hetero-structure, which is further proved by regulating $Sr(OH)_2$ concentration of hydrothermal solution. The XRD patterns of the resulting TSr_{300}/Ti, TSr_{301}/Ti, TSr_{302}/Ti (corresponding to 0.010 M, 0.025 M, 0.050 M $Sr(OH)_2$ hydrothermal solution) and the reference TSr_0/Ti and Ti samples are revealed in Fig. 1b. Compared with the reference samples, these XRD patterns, which along with anatase TiO_2 (101), (004), (200), (105), (211), (204), (115) facets and perovskite $SrTiO_3$ (110), (200), (211), (220)

facets, displays inconsistent variation for these hetero-structured samples. With $Sr(OH)_2$ concentration from 0 M to 0.010 M and 0.025 M, 0.050 M, the XRD patterns of the resulting TSr_{300}/Ti show no evident difference compared with the reference TSr_0/Ti, however, the resulting TSr_{301}/Ti, TSr_{302}/Ti with oriented-growth {001} facet of anatase TiO_2 are signified by XRD patterns. What is worth mentioning, anatase TiO_2 {101} peak can be measured from these resulting hetero-structured sample except for TSr_{301}/Ti, which probably results from the characteristic features of XRD and FE-TEM measurements.

In addition, the resulting hetero-structured sample TSr_{30}*/Ti annealing at 250 °C (See Fig. S1) reveals poor crystallize because of no characteristic diffraction peaks of anatase TiO_2 and weak variation of peak intensity of perovskite $SrTiO_3$ compared to the resulting sample TSr_{301}*/Ti without annealing. With the increasing temperature to 450 °C, the preferential oriented-growth anatase TiO_2 {001} facet can be definitely measured by XRD measurement (See Fig. 1). From the above results, the fabrication of the hetero-structured film with preferential oriented-growth {001} facet of anatase TiO_2 is probably attributed to the synergistic effect of the formation of $SrTiO_3$ on the "structure" TiO_2 nanotubes and the appropriate annealing treatment, and the in-situ substitution of the suitable content Sr to Ti on the surface of TiO_2 nanotubes probably impels the preferential growth of anatase TiO_2 {001} facet after the annealing.

To confirm the topographic features of the hetero-structured sample, these samples are further characterized by FE-SEM and FE-TEM. In Fig. 2, FE-SEM views with EDX spectra of the hetero-structured TSr_{301}/Ti and reference TSr_0/Ti samples are showed, respectively. The cross-section views of these samples reveal similar morphology in Fig. 2a and Fig. 2d, their corresponding magnifying views from the selected area, however, indicate wide difference in Fig. 2b and Fig. 2e, and compared to the bamboo-shaped nanotubes with small "ripples" for the

reference TSr_0/Ti sample,[39, 40] the numerous "small gibbosity" distribute uniformly on the surface of nanotubes and thus the steep surface is fabricated for the hetero-structured sample,[32, 34, 36] which is originated form the $SrTiO_3$ particles precipitation on the surface of TiO_2 nanotubes in a hydrothermal dissolution-precipitation process.[35, 37] Meanwhile, the EDX spectra of the hetero-structured and reference sample also confirm the existence of Ti, O, Sr elements in Fig. 2c and Ti, O elements in Fig. 2f, respectively. In addition, SEM views of the template TSr_0*/Ti sample (See Fig. S2, Supporting Information) show that the precipitation from the reactive system is attached on the top of TiO_2 nanotubes and these anodizing nanotubes are closely connected with the Ti substrate before hydrothermal treatment.

In Fig. 3, FE-TEM views of the hetero-structured TSr_{301} indicate that the fabricating $SrTiO_3$ attach and overlap over the "structure-directed" TiO_2 nanotubes, and the measurement from the several selected areas in Fig. 3a determinately manifest the preferential growth of anatase TiO_2 {001} facet and the mixed phases of $SrTiO_3$ and TiO_2. In Fig. 3b, high-resolution FE-SEM view signifies that the lattice spacing of the selected area A is 0.234 nm and 0.346 nm with their interfacial angle 69.3°, which is identified as the {001} and {101} facet of anatase TiO_2,[2, 41, 42]and the slight difference of the interfacial angle is probably caused by the $SrTiO_3$ fabrication of in-situ Sr substitution for Ti on the surface of TiO_2 nanotubes. In Fig. 3c, the electron diffraction patters of selected area B point out the presence of anatase TiO_2 (004), (211) facet with the interfacial angle 79.6° and further confirm that anatase TiO_2 nanotubes with {001} facet preferred growth is a single-crystal-like crystal. Nevertheless, high-resolution FE-TEM views of TSr_0 (reference TiO_2 nanotube) and its corresponding SEAD patters in Fig. S3 (See Supporting Information) demonstrate that the reference sample is polycrystalline in good correspondence with the XRD result of Fig. 1 and the published work.[4, 43] In Fig. 3d-e, the lattice spacing of

high-resolution FE-TEM views is 0.275 nm and the corresponding FFT in the inset of Fig. 3d indicates the lattice spacing 0.275 nm with the interfacial angle 60°, which is good accordance with cubic $SrTiO_3$ (011), (110), (101) facet with their intersection angle, and this magnifying hetero-structured junction with the lattice spacing is 0.235 nm, 0.276 nm is also identified in Fig. 2f, and, thereby, prove the hetero-structured existence of the preferred growth {001} facet of anatase TiO_2 and the (110) facet of cubic $SrTiO_3$ based on the above. These results definitely demonstrate the preferential growth of anatase TiO_2 {001} facet and the formation of TiO_2 and $SrTiO_3$ phase in the hetero-structured sample, which is perfectly coincident with the XRD patterns.

In Fig. S4 (See Supporting Information), FE-TEM views of the hetero-structured TSr_{302} also reveal that Sr is substituted for Ti to fabricate $SrTiO_3$ particles and, thus, bond and superpose on the surface of TiO_2 nanotubes, and FE-TEM views of the selected areas and EDX spectrum are definitely demonstrate the preferred-growth {001} facet of anatase TiO_2 and the hetero-structured existence. In Fig. S4b, high-resolution FE-TEM view of the selected area B indicates the lattice spacing 0.346 nm, 0.469 nm with their corresponding interfacial angle 68.8° and the lattice spacing 0.349 nm, 0.469 nm with their angle 68.5°, which accord with the {101} and {001} facet of anatase TiO_2. In Fig. S4c, high-resolution FE-TEM view of the selected area C points out the lattice spacing 0.275 nm consistent with perovskite $SrTiO_3$ {110} facet. In addition, the EDX spectrum of Fig. S4d reveals the elemental composition Ti, Sr, O of the sample (Cu element from the measurement).

Fig. 4 shows the XPS spectra of the hetero-structured TSr_{301}/Ti, TSr_{301}*/Ti and reference TSr_0/Ti, TSr_0*/Ti samples. Their full spectra (See Fig. 4a) reveal that the peak of F1s exists in the TSr_{301}*/Ti, TSr_0*/Ti sample and disappears in the TSr_{301}/Ti, TSr_0/Ti sample, which results

from F^- ions of NH_4F in the anodizing electrolyte system, and the peak of F1s almost disappears when the annealing temperature increases to 450 °C. Fig. 4 b-d indicate Ti 2p, O 1s, Sr 3d spectra in the TSr_{301}/Ti sample and their corresponding peaks at 458.91 eV and 464.55 eV for Ti 2p, 529.82 eV and 531.55 eV for O1s, 132.77 eV and 134.10 eV for Sr 3d,[30, 33, 43, 44] respectively. Based on the above XRD, FE-SEM, FE-TEM and XPS measurement, TiO_2 nanotubes overwhelmingly dominate the hetero-structured samples and the following Raman spectra of the hetero-structured TSr_{301}/Ti and reference TSr_0/Ti sample (See Fig. S5, Supporting Information) further certify this point. The reference $TiSr_0$/Ti sample exhibits characteristic peaks of six phonon scattering modes (A_{1g} + 2 B_{1g} + 3E_{1g}) of crystalline anatase,[12, 45-47] the modes E_g (1)、E_g (2)、B_{1g} (1)、A_{1g}+B_{1g} (2)、E_g (1) are indexed to the peaks at about 153 cm^{-1}、206 cm^{-1}、404 cm^{-1}、526 cm^{-1}、645 cm^{-1}, the difference of resonant frequency between A_{1g} and B_{1g} (2) band is only 6 cm^{-1} and they usually overlap in these spectra. Likewise, the Raman spectrum of the hetero-structured TSr_{30}/Ti sample also illuminates the six similar phonon scattering modes (A_{1g} + 2 B_{1g} + 3E_{1g}) with the site at 151 cm^{-1}、204 cm^{-1}、404 cm^{-1}、524 cm^{-1}、642 cm^{-1}, which is similar to those of the TSr_0/Ti sample, and the broadening and offset of these scattering peaks appear compared to those of TSr_0/Ti sample, which is probably ascribed to the partial conversion of TiO_2 to $SrTiO_3$ on the surface of the TiO_2 nanotubes. In addition, the hetero-structured and reference samples are measured to investigate their photoelectrochemical properties. In Fig. S6, the curves of CV and LSV points out the peak value at about 0.5 v and their corresponding currents at this voltage is about 0.00318 A, 0.00138 A, respectively. Compared to the reference TSr_0/Ti electrode, the hetero-structured TSr_{301}/Ti electrode with the higher current is probably attributed to excite the transference electrons from the conduction bands (CB) of $SrTiO_3$ to the CBs of TiO_2 under the appropriate applied voltage.

The photocatalytic and photoelectrocatalytic decoloration of MB solution are implemented to evaluate their activities of the hetero-structured samples. Fig. 5a-b show the photocatalytic, photoelectrocatalytic decoloration of MB solution using the hetero-structured TSr_{300}/Ti, TSr_{301}/Ti, TSr_{302}/Ti, TSr_{301}*/Ti and reference TSr_0/Ti catalysis and their corresponding pseudo-first-order kinetics. With the reaction time to 120 min, the photocatalytic efficiency of decoloring MB solution is about 59.87%, 93.92%, 83.92%, 18.00%, 50.34% and 1.68% corresponding to the hetero-structured TSr_{300}/Ti, TSr_{301}/Ti, TSr_{302}/Ti, TSr_{301}*/Ti, reference TSr_0/Ti samples and Blank, and the adsorption spectra of TSr_{301}/Ti and reference TSr_0/Ti with different reaction time (See Fig. S7, Supporting Information) is also verified this result, these according reaction-rate constants are 0.00750 min^{-1}, 0.02302 min^{-1}, 0.01536 min^{-1}, 0.00575 min^{-1}, 0.00169 min^{-1}, 6.55884 E^{-5} min^{-1}, respectively. Likewise, the photoelectrocatalytic reaction (0.5V) of decolorizing MB solution also exhibits the catalytic activities of the hetero-structured samples. With the time from 0 to 15 min, the decolorizing efficiency of the hetero-structured TSr_{301}/Ti, TSr_{302}/Ti catalysts soars to 99.66%, 97. 69%, the hetero-structured TSr_{300}/Ti with the efficiency of 68.66% manifests almost equivalent activities to the reference TSr_0/Ti with that of 63.77%, the hetero-structured TSr_{301}*/Ti, however, displays the lowest activity with the efficiency of 28.00%, and the reaction-rate constants are 0.04662 min^{-1}, 0.38492 min^{-1}, 0.26143 min^{-1}, 0.04214 min^{-1}, 0.01273 min^{-1}, 3.61447 E^{-4} min^{-1} corresponding to the hetero-structured TSr_{300}/Ti, TSr_{301}/Ti, TSr_{302}/Ti, TSr_{301}*/Ti, reference TSr_0/Ti samples and Blank, and the adsorption spectra of TSr_{301}/Ti and reference TSr_0/Ti are further verified the photoelectrocatalytic result (See Fig. S8, Supporting Information).

The above photocatalytic and photoelectrocatalytic results reveal the accordant tendency for the catalytic activities of hetero-structured samples, and the applied voltage can extraordinary

improve their catalytic performance. Compared with the hetero-structured TSr_{300}/Ti, TSr_{301}*/Ti and reference TSr_0/Ti, the catalytic properties of the hetero-structured TSr_{301}/Ti and TSr_{302}/Ti are mostly attributed to the dominant high-reactive {001} facet of anatase TiO_2 and the junction interface of mixed phases TiO_2 and $SrTiO_3$ in the hetero-structured samples. High-reactive anatase TiO_2 {001} facet improves the effective separation of photo-generated electron-hole pairs and increase the electron diffusion length in the photocatalytic process,[17, 25, 38, 48-50] and the transference electrons of junction interface generate the electrons flow and then cause an efficient spatial separation of electron-hole pairs. [30, 32] Based on the catalytic activities and characterizations, the activity of hetero-structured TSr_{300}/Ti is probably described to the phase composition similar to the reference TSr_0/Ti, and the activity of TSr_{301}*/Ti is probably distributed to the contribution of perovskite $SrTiO_3$. Especially, with the increasing concentration of $Sr(OH)_2$ solution, the hetero-structured TSr_{301}/Ti with the best photocatalytic activity is attributed to the synergetic effect of the high-reactive anatase TiO_2 {001} facet and the positive coupling of $SrTiO_3$ and TiO_2 phases, and the positive cooperation derives from the appropriate coverage of in-situ fabricating $SrTiO_3$ on the "structure-directed" TiO_2 nanotubes in the dissolution-precipitation process and, thus, increases the accessibility of the active sites of TiO_2 nanotubes surface to favor charge carriers transfer. [35, 44]

In summary, we report a simple hydrothermal method to synthesize the hetero-structured TSr nanotube array film with the oriented-growth {001} facet of anatase TiO_2 nanotubes attached on a Ti substrate, and the $SrTiO_3$ fabrication on the surface of TiO_2 nanotubes by a dissolution-precipitation process and the following appropriate annealing directly impel the preferential growth of high-reactive {001} facet during anatase TiO_2 crystal growth. Furthermore, this hetero-structured film reveals the improved photocatalytic and photoelectrochemical activities

compared with the reference TiO_2 nanotubes, and these result is probably caused by the synergistic effects: (1) The high-reactive {001} facets effectively accelerate the transfer mechanism of photo-generated charges in the hetero-structured nanotubes, (2) The hetero-structured interface plays a positive role in suppressing the photo-generated charges combination of the heterojuction. More importantly, this work, here, provides a new strategy to synthesis the coupling of TiO_2 and perovskite ABO_3 ($SrTiO_3$, $BaTiO_3$, $CaTiO_3$ etc.) with controllable high-reactive facets, and further utilize the synergy mechanism of high-active facet and the junction interface to enhance their photo-electrochemical, photovoltaic performance and, thereby, expand their application in those related fields.

ACKNOWLEDGMENTS

This work was supported by National Basic Research Program of China (973 program, No. 2012CB720100, No. 2014CB239300), Science Foundation for the Excellent Youth Scholars of Ministry of Education of China (No. 20130032120019), and China Postdoctoral Science Foundation of China (No. 2013M541180), Natural Science Foundation of Tianjin (No. 13JCQNJC05700).

† **Supporting Information**. Details of experimental section; FE-TEM view of the reference TSr_0 and hetero-structured TSr_{302} sample, Raman Spectra of the hetero-structured TSr_{301}/Ti and reference TSr_0/Ti samples, CV and LSV curves of the hetero-structured TSr_{301}/Ti and reference TSr_0/Ti samples, and the adsorption spectra of MB solution over the hetero-structured and reference TSr_0/Ti samples.

REFERENCES

1 H. Xu, P. Reunchan, S. Ouyang, H. Tong, N. Umezawa, T. Kako and J. Ye, *Chem. Mater.*, 2013, 25, 405-411.

2 N. Roy, Y. Sohn and D. Pradhan, *Acs Nano*, 2013, 7, 2532-2540.
3 Z. Zhang, L. Zhang, M. N. Hedhili, H. Zhang and P. Wang, *Nano Lett.*, 2013, 13, 14-20.
4 J. R. Huang, X. Tan, T. Yu, L. Zhao and S. Xue, *Rsc Adv.*, 2012, 2, 12657-12660.
5 K. L. Li, Z. B. Xie and S. Adams, *Electrochimi. Acta*, 2012, 62, 116-123.
6 Y. Y. Song, F. Schmidt-Stein, S. Bauer and P. Schmuki, *J. Am. Chem. Soc.*, 2009, 131, 4230-4232.
7 Z. X. Su and W. Z. Zhou, *J. Mater. Chem.*, 2011, 21, 8955-8970.
8 M. Lazzeri, A. Vittadini and A. Selloni, *Phys. Rev. B*, 2001, 63, 155409.
9 M. Lazzeri, A. Vittadini and A. Selloni, *Phys. Rev. B*, 2002, 65, 119901.
10 H. G. Yang, C. H. Sun, S. Z. Qiao, J. Zou, G. Liu, S. C. Smith, H. M. Cheng and G. Q. Lu, *Nature*, 2008, 453, 638-U634.
11 L. Sun, Z. L. Zhao, Y. C. Zhou and L. Liu, *Nanoscale*, 2012, 4, 613-620.
12 A. S. Ichimura, B. M. Mack, S. M. Usmani and D. G. Mars, *Chem. Mater.*, 2012, 24, 2324-2329.
13 W. Yang, J. Li, Y. Wang, F. Zhu, W. Shi, F. Wan and D. Xu, *Chem. Commun.*, 2011, 47, 1809-1811.
14 J. S. Chen, Y. L. Tan, C. M. Li, Y. L. Cheah, D. Luan, S. Madhavi, F. Y. C. Boey, L. A. Archer and X. W. Lou, *J. Am. Chem. Soc.*, 2010, 132, 6124-6130.
15 G. Liu, C. Sun, H. G. Yang, S. C. Smith, L. Wang, G. Q. Lu and H. M. Cheng, *Chem. Commun.*, 2010, 46, 755-757.
16 Y. Alivov and Z. Y. Fan, *J. Phys. Chem. C*, 2009, 113, 12954-12957.
17 M. M. Maitani, K. Tanaka, D. Mochizuki and Y. Wada, *J. Phys. Chem. Lett.*, 2011, 2, 2655-2659.
18 H. Xu, S. Ouyang, P. Li, T. Kako and H. J. Ye, *ACS Appl. Mater. Inter.*, 2013, 5, 1348-1354.
19 J. Pan, G. Liu, G. Q. Lu and H. M. Cheng, *Angew. Chem. Int. Edit.*, 2011, 50, 2133-2137.
20 B. X. Y. M. Y Xing, H. Yu, B. Z. Tian, S. Bagwasi, J. L. Zhang and X. Q. Gong, *J. Phys. Chem. Lett.*, 2013, 4, 3910-3917.
21 Z. Zhao, Z. Sun, H. Zhao, M. Zheng, P. Du, J. Zhao and H. Fan, *J. Mater. Chem.*, 2012, 22, 21965-21971.
22 X. Han, B. Zheng, J. Ouyang, X. Wang, Q. Kuang, Y. Jiang, Z. Xie and L. Zheng, *Chem.- Asian J.*, 2012, 7, 2538-2542.
23 X. Han, X. Wang, S. Xie, Q. Kuang, J. Ouyang, Z. Xie and L. Zheng, *Rsc Adv.*, 2012, 2, 3251-3253.
24 Z. Zhao, H. Tan, H. Zhao, D. Li, M. Zheng, P. Du, G. Zhang, D. Qu, Z. Sun and H. Fan, *Chem. Commun.*, 2013, 49, 8958-8960.
25 S. Lee, I. J. Park, D. H. Kim, W. M. Seong, D. W. Kim, G. S. Han, J. Y. Kim, H. S. Jung and K. S. Hong, *Energy Environ. Sci.*, 2012, 5, 7989-7995.
26 M. H. Jung, M. J. Chu and M. G. Kang, *Chem. Commun.*, 2012, 48, 5016-5018.
27 S. Li, J. Chen, F. Zheng, Y. Li and F. Huang, *Nanoscale*, 2013, 5, 12150-12155.
28 R. Li, Q. Li, L. Zong, X. Wang and J. Yang, *Electrochimi. Acta*, 2013, 91, 30-35.
29 J. Tian, Y. Sang, Z. Zhao, W. Zhou, D. Wang, X. Kang, H. Liu, J. Wang, S. Chen, H. Cai and H. Huang, *Small*, 2013, 9, 3864-3872.
30 J. Ng, S. Xu, X. Zhang, H. Y. Yang and D. D. Sun, *Adv. Funct. Mater.*, 2010, 20, 4287-4294.
31 Y. Yang, K. Lee, Y. Kado and P. Schmuki, *Electrochem. Commun.*, 2012, 17, 56-59

32 J. Zhang, J. H. Bang, C. C. Tang and P. V. Kamat, Acs Nano, 2010, 4, 387-395.
33 X. M. Zhang, K. F. Huo, L. S. Hu, Z. W. Wu and P. K. Chu, *J. Am. Ceram. Soc.*, 2010, 93, 2771-2778.
34 Y. Zhang, Y. Bu, J. Yu and P. Li, *J. Nanopart. Res.*, 2013, 15, 1717.
35 C.W. Kim, M. J. Choi, Y. S. Kang and Y. S. Kang, *J. Mater. Chem. A*, 2013, 1, 11820-11827
36 Z. Jiao, T. Chen, J. Xiong, T. Wang, G. Lu, J. Ye and Y. Bi, *Sci. Rep.-UK*, 2013, 3, 2720.
37 Y. Xin, J. Jiang, K. Huo, T. Hu and P. K. Chu, *Acs Nano*, 2009, 3, 3228-3234.
38 M. H. Jung, M. J. Chu and M. G. Kang, *Chem. Commun.*, 2012, 48, 5016-5018.
39 S. Q. Li, G. M. Zhang, D. Z. Guo, L. G. Yu and W. Zhang, *J. Phys. Chem. C*, 2009, 113, 12759-12765.
40 Q. W. Chen and D. S. Xu, *J. Phys. Chem. C*, 2009, 113, 6310-6314.
41 D. Wu, Z. Gao, F. Xu, J. Chang, S. Gao and K. Jiang, *Crystengcomm*, 2013, 15, 516-523.
42 W. Wang, C. Lu, Y. Ni and Z. Xu, *Crystengcomm*, 2013, 15, 2537-2543.
43 H. Bai, J. Juay, Z. Liu, X. Song, S. S. Lee and D. D. Sun, *Appl. Catal. B-Environ.*, 2012, 125, 367-374.
44 P. T. Cao, J. Y. Li, H. C. Wang, L. C. Shao and C. Y. Liu, *Langmuir*, 2011, 27, 2946-2952.
45 J. Felipe Montoya, I. Ivanova, R. Dillert, D. W. Bahnemann, P. Salvador and J. Peral, *J. Phys. Chem. Lett.*, 2013, 4, 1415-1422.
46 M. Giarola, A. Sanson, F. Monti, G. Mariotto, M. Bettinelli, A. Speghini and G. Salviulo, *Phys. Rev. B*, 2010, 81,174305.
47 F. Tian, Y. Zhang, J. Zhang and C. Pan, *J. Phys. Chem. C*, 2012, 116, 7515-7519.
48 X. C. Ma, Y. Dai, M. Guo and B. B. Huang, *J. Phys. Chem. C*, 2013, 117, 24496-24502.
49 C. Liu, X. Han, S. Xie, Q. Kuang, X. Wang, M. Jin, Z. Xie and L. Zheng, *Chem.- Asian J.*, 2013, 8, 282-289.
50 W. Q. Fang, X. Q. Gong and H. G. Yang, *J. Phys. Chem. Lett.*, 2011, 2, 725-734.

Figure Captions:

Fig. 1 XRD patterns of the hetero-structured TSr_{301}/Ti, TSr_{30}*/Ti and reference TSr_0/Ti, Ti substrate (a) and TSr_{300}/Ti, TSr_{301}/Ti, TSr_{302}/Ti and reference TSr_0/Ti, Ti substrate (b).

Fig. 2 FE-SEM views and their corresponding EDX of the TSr_{301}/Ti (a, b, c) and reference TSr_0/Ti (d, e, f) sample.

Fig. 3 FE-TEM views of the hetero-structured TSr_{301} sample. (a) Low-resolution FE-TEM view of the TSr_{30} sample with several selected areas. (b) High-resolution FE-TEM view of the selected area A and identified as {001}, {101} facet with their interfacial angle 69.3 ^{o}. (c) The SAED patters of the selected area B and identified as a single-crystal-like TiO_2 nanotube and their angle 79.6^{o} of anatase TiO_2 (004) and (211) facet. (d, e) High-resolution FE-TEM views of the selected areas d, e and identified as {110} facet, the inset of (d) with $SrTiO_3$ (011), (110), (101) facets and their interfacial angles 60^{o}. (f) The interface of heterojuction with TiO_2 {001} and $SrTiO_3$ {110} facet.

Fig. 4 XPS spectra of the hetero-structured TSr_{301}/Ti, TSr_{301}*/Ti and reference TSr_0/Ti, TSr_0*/Ti samples. (a) The full spectra of the TSr_0*/Ti (1), TSr_0/Ti (2), TSr_{301}*/Ti (3), TSr_{301}/Ti (4) samples. (b, c, d) The Ti 2p, O1s, Sr 3d, F1s spectra of the hetero-structured TSr_{301}/Ti sample.

Fig. 5 (a, b) The photocatalytic decoloration of MB solution using the hetero-structured TSr_{300}/Ti, TSr_{301}/Ti, TSr_{302}/Ti, TSr_{301}*/Ti, reference TSr_0/Ti samples and their pseudo-first-order kinetics; (c, d) The photoelectrocatalytic decoloration of MB solution using the hetero-structured TSr_{300}/Ti, TSr_{301}/Ti, TSr_{302}/Ti, TSr_{301}*/Ti, reference TSr_0/Ti samples and their pseudo-first-order kinetics. The blank experiment is also showed

Fig 1

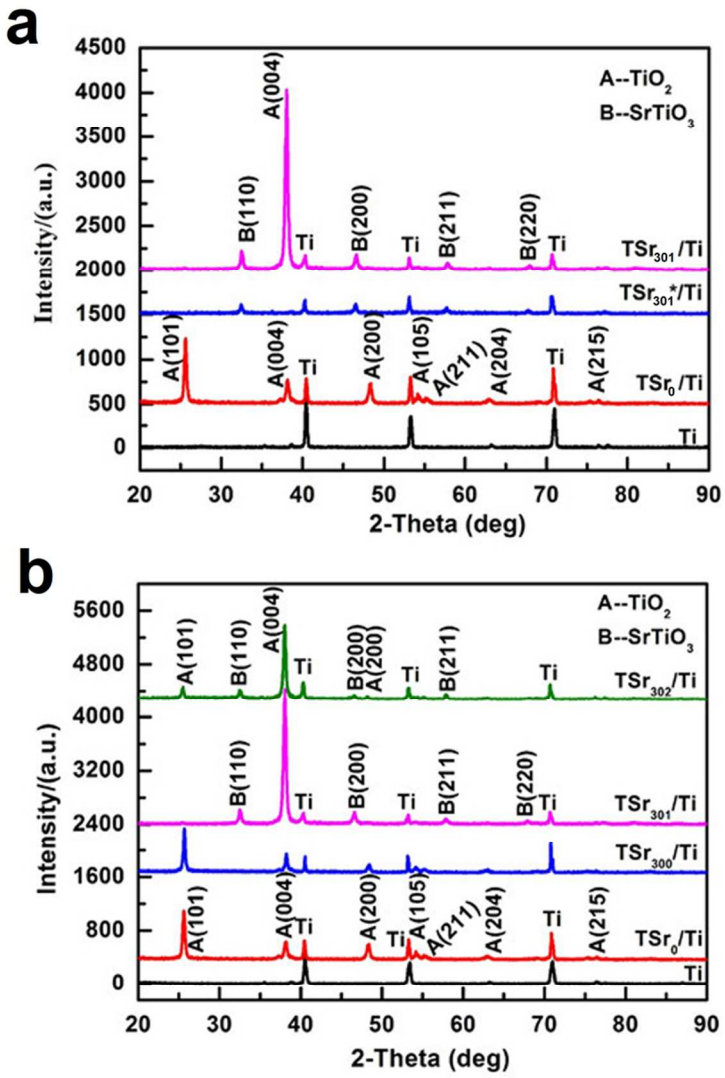

Fig 2

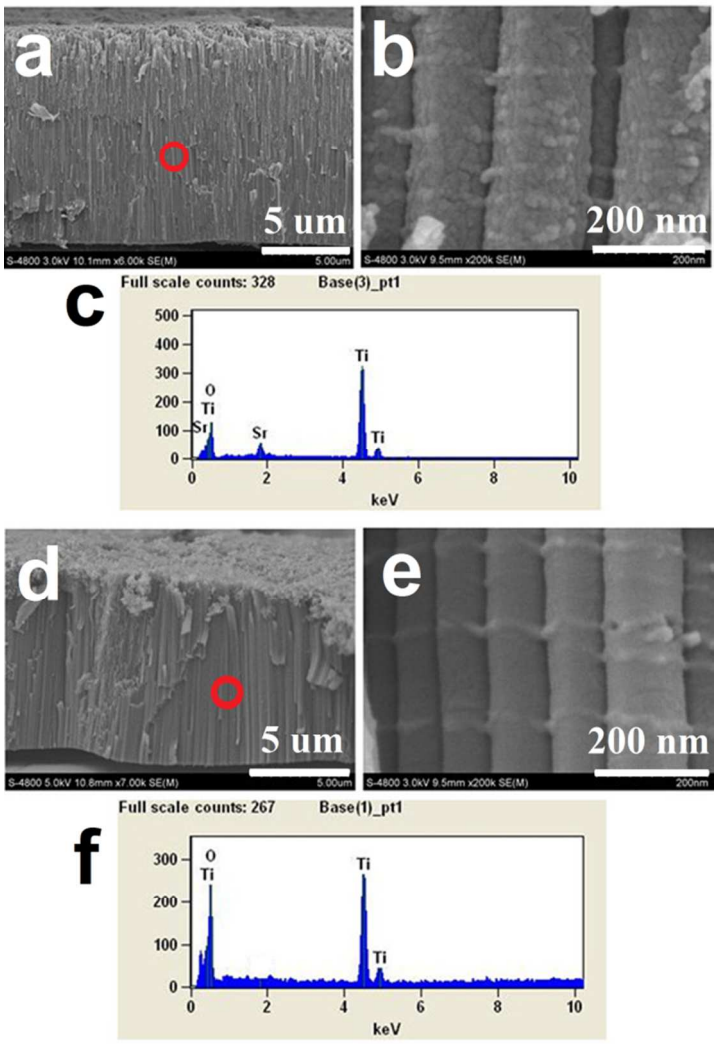

Fig 3

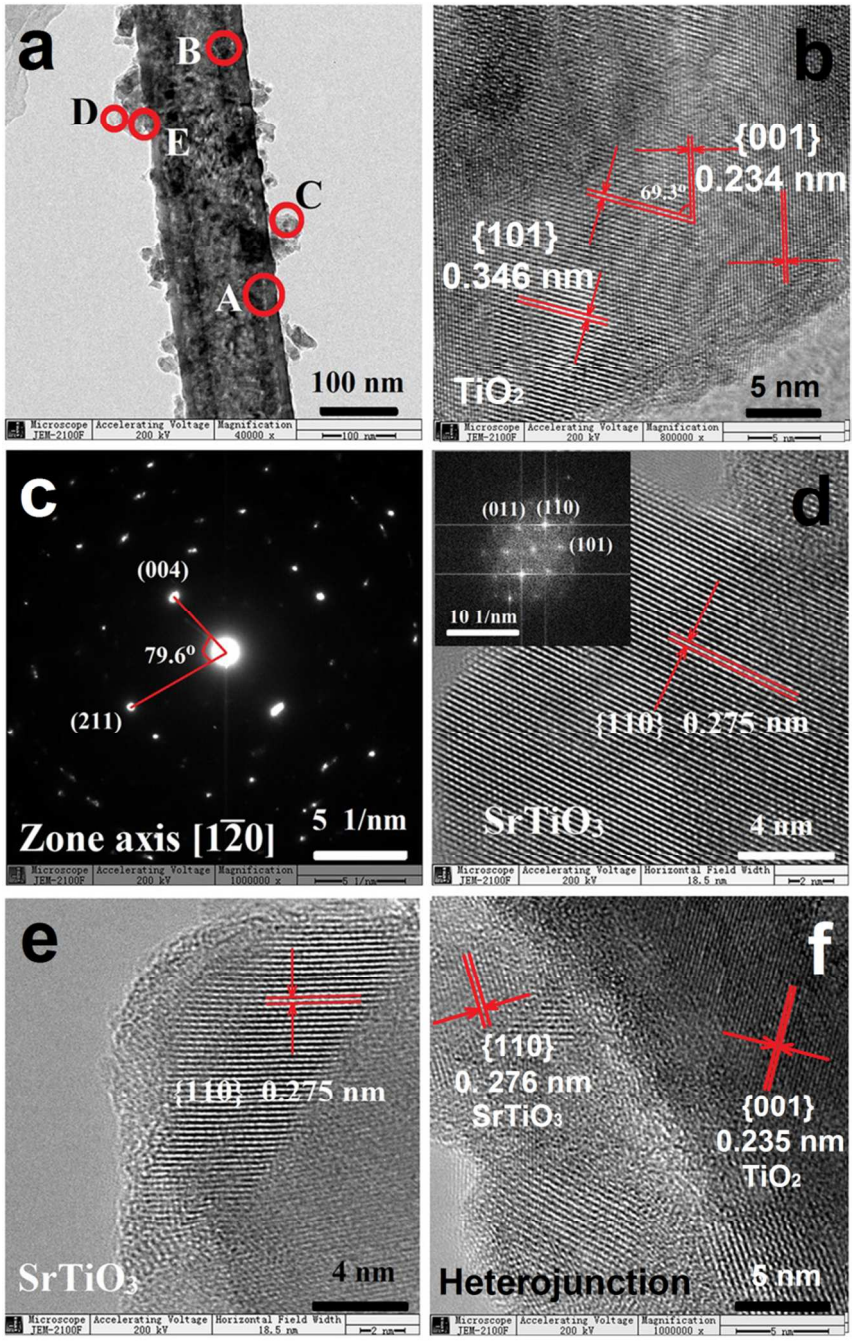

Fig 4

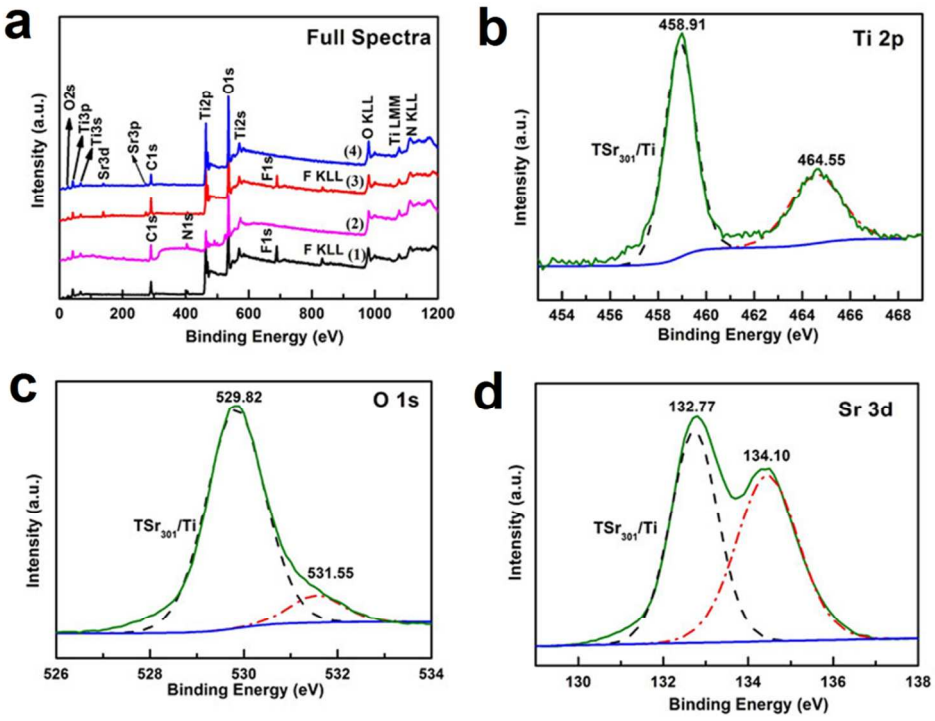

Fig 5